nature physics

Article

https://doi.org/10.1038/s41567-024-02541-w

Collective flow of fermionic impurities immersed in a Bose-Einstein condensate

Received: 25 April 2023

Accepted: 14 May 2024

Published online: 21 June 2024

Check for updates

Zoe Z. Yan © 1,2, Yiqi Ni¹, Alexander Chuang¹, Pavel E. Dolgirev © 3,4, Kushal Seetharam 9^{3,5}, Eugene Demler⁴, Carsten Robens 9¹&

Interacting mixtures of bosons and fermions are ubiquitous in nature. They form the backbone of the standard model of physics, provide a framework for understanding quantum materials and are of technological importance in helium dilution refrigerators. However, the description of their coupled thermodynamics and collective behaviour is challenging. Bose-Fermi mixtures of ultracold atoms provide a platform to investigate their properties in a highly controllable environment, where the species concentration and interaction strength can be tuned at will. Here we characterize the collective oscillations of spin-polarized fermionic impurities immersed in a Bose-Einstein condensate as a function of the interaction strength and temperature. For strong interactions, the Fermi gas perfectly mimics the superfluid hydrodynamic modes of the condensate, from low-energy quadrupole modes to high-order Faraday excitations. With an increasing number of bosonic thermal excitations, the dynamics of the impurities cross over from the collisionless to the hydrodynamic regime, reminiscent of the emergence of hydrodynamics in two-dimensional electron fluids.

The paradigmatic example of fermions coupled to a bosonic bath is the motion of itinerant electrons through an ionic crystal. The coupling to the ionic lattice vibrations endows the electrons with a shifted energy and mass, as they become dressed into polarons^{1,2}, the first instance of the quasiparticle concept. We also encounter Bose-Fermi mixtures as dilute solutions of fermionic ³He in bosonic superfluid ⁴He (ref. 3), in quark-meson models in high-energy physics⁴ and in two-dimensional electronic materials, where interactions between excitons and electrons can be controlled⁵⁻⁷. Ultracold atomic gases provide arguably the purest realizations of Bose-Fermi mixtures, featuring precisely understood, tunable short-range interactions and a high degree of experimental control⁸⁻²¹, offering a direct comparison with theoretical models^{22–26}. In recent years, atomic Bose–Fermi mixtures enabled the study of dual superfluids²⁷⁻³¹, the onset of phase separation and

mean-field collapse^{12,13,19,32,33}, and the observation of strong-coupling Bose polarons^{34,35}.

The general dynamics of fermions interacting with a partially condensed Bose gas at finite temperature are challenging to describe, as interactions between fermions and bosons come in two flavours. On the one hand, fermions can incoherently scatter with thermal bosons, leading to momentum-changing collisions. On the other hand, fermions also experience momentum-preserving interactions, in particular with the Bose-Einstein condensate (BEC), in the form of an effective potential^{22,36-39}. The interplay between the two types of interaction dictates the dynamics of the whole system 40-50. Most challenging is the regime for strong interactions where the non-superfluid system crosses over from collisionless to the collisionally hydrodynamic regime. Such a regime is observed in electron-phonon mixtures in the context of

MIT-Harvard Center for Ultracold Atoms, Research Laboratory of Electronics, and Department of Physics, Massachusetts Institute of Technology, Cambridge, MA, USA. 2Physics Department and James Franck Institute, University of Chicago, Chicago, IL, USA. 3Department of Physics, Harvard University, Cambridge, MA, USA. 4Institute for Theoretical Physics, ETH Zurich, Zurich, Switzerland. 5Department of Electrical Engineering, Massachusetts Institute of Technology, Cambridge, MA, USA. Me-mail: zwierlei@mit.edu

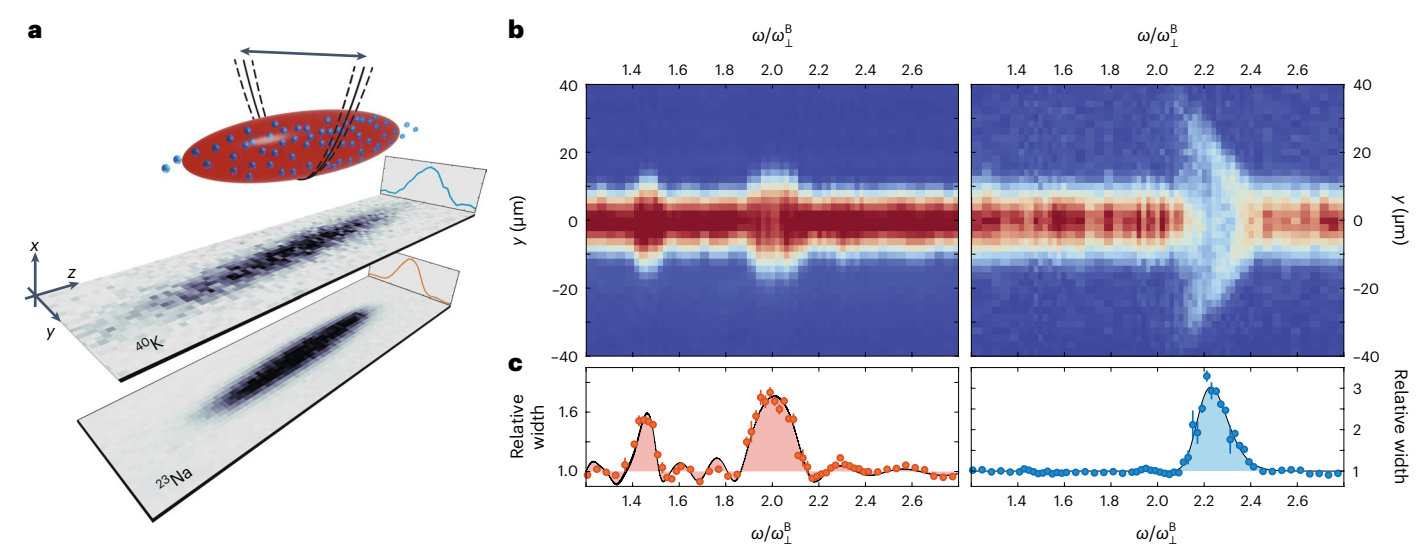


Fig. 1| **Collective oscillations in a Bose–Fermi mixture. a**, Illustration of a dilute gas of fermions (blue) immersed in a Bose–Einstein condensate (red), both trapped in an optical potential. In situ absorption images of the fermionic 40 K and bosonic 23 Na are shown beneath. Radial collective oscillations are induced by periodically modulating the depth of the optical potential. **b**, The doubly integrated line densities along the transverse (y) direction of the boson (left) and fermion (right) clouds as a function of modulation frequency ω , at

zero interspecies interaction ($a_{\rm BF}$ = 0). **c**, Spectra of the uncoupled Bose–Fermi system, showing the boson (left, red circles) and fermion (right, blue circles) relative widths, reveal the superfluid hydrodynamic response of the BEC and the response of the non-interacting, near-degenerate gas of spin-polarized fermions. The solid black lines show predictions from the hydrodynamic scaling ansatz in equation (1) and a phenomenological Gaussian fit, respectively. All error bars show the standard error of the mean.

high-temperature superconductivity^{51,52}. With such strong interactions and with bosons partially condensed, the question arises whether the system indeed remains superfluid, with fermions flowing without dissipation through the condensate. Also, it is unclear how thermal bosonic excitations alter the transport properties of fermions. In this Article, we thoroughly address these questions, observing collective flow of fermionic impurities mimicking closely the superfluid hydrodynamic modes of the condensate. Despite strong interspecies interactions the flow can be modelled as collisionless and driven by the condensate's mean field. With increasing temperature, we observe a crossover to collision-dominated hydrodynamic flow.

Collective excitations are exquisitely sensitive probes of interparticle scattering and interactions. They have been used to demonstrate the superfluid hydrodynamic flow of BECs $^{53-55}$ and collisional hydrodynamics in interacting Fermi gases $^{56-62}$. Collective oscillations have also been measured in coupled Bose–Fermi superfluids 27,28,30,31 and in Bose–Fermi mixtures 20,21,33,63,64 , revealing phenomena such as collisional hydrodynamics in thermal mixtures 63 , collisionless uncoupled dipole oscillations in degenerate mixtures 63 , and sound propagation 21 . Here we study a novel regime—the limit of a dilute gas of spin-polarized fermions immersed in a BEC—as relevant for the physics of Bose polarons 34,35 and unconventional superconductors with low carrier densities 65 .

We probe collective excitations of 40 K fermions and a 23 Na BEC as a function of drive frequency and across a range of Bose–Fermi interactions, revealing the energy and spectral width of low-lying excitations. The experiment starts with an ultracold near-degenerate gas of fermionic 'impurity' atoms immersed in the BEC, both held in a 1,064 nm crossed optical dipole trap with near-cylindrical symmetry (Fig. 1a). For our coldest samples, we evaporatively cool both species to $T \approx 30$ nK, corresponding to $T/T_c \lesssim 0.2$ and $T/T_F \approx 0.6$, where $T_{c(F)}$ is the condensate's critical temperature (the Fermi temperature). Both species are in their respective hyperfine ground states. We control the interspecies interactions by ramping the magnetic field near Feshbach resonances, allowing us to continuously tune the s-wave scattering length, a_{BF} . The typical peak boson density is $n_B = 7 \times 10^{13}$ cm⁻³, and the typical impurity concentration varies between $n_F/n_B \approx 0.003$ and 0.02 (Methods). We characterize the low-energy radial excitations

of the mixture at varying interspecies interaction strengths. Modulating the radial trapping potential depth at frequency ω for ten cycles, we measure the in situ width of the clouds (Fig. 1a) The number of cycles N allows for spectral resolution $-\omega/N$, while the probe time is kept short compared with the mixture's lifetime, limited by three-body loss. When the modulation excites a resonant mode of either species, the cloud's width expands radially. Figure 1b,c depicts the bosonic and fermionic spectrograms for a decoupled mixture at $a_{BF} = 0$. Two resonances are observed in the BEC at $\sqrt{2}\omega_{\perp}^{\rm B}$ and $2\omega_{\perp}^{\rm B}$, while only one fermionic resonance is excited at $2\omega_{\nu}^{F}$. Here, $\omega_{\perp}^{B} = (\omega_{x}^{B}\omega_{y}^{B})^{1/2}$ is the bosons' geometric mean radial trapping frequency, and ω_{ν}^{F} is the fermions' trap frequency along the transverse y direction, with the two frequencies related by $\omega_{\nu}^{\rm F} = 1.16 \,\omega_{\perp}^{\rm B}$ (Supplementary Information). The BEC obeys superfluid hydrodynamics, which couples the two collisionless radial modes, giving rise to a quadrupole (out-of-phase) and a breathing (in-phase) resonance at $\sqrt{2\omega_{\perp}^{B}}$ and $2\omega_{\perp}^{B}$, respectively ^{66,67}. Across all frequencies, the bosonic spectral response is well captured using a hydrodynamic scaling ansatz⁶⁸ (Supplementary Information and Fig. 1c, red shaded area):

$$\ddot{b}_i + \omega_i^{\rm B}(t)^2 b_i - \frac{\omega_i^{\rm B}(0)^2}{b_i \prod_j b_j} = 0,$$
 (1)

where $i \in (x, y, x)$ and b_i is the dimensionless scaling parameter of the BEC's Thomas–Fermi radius in the ith direction. The spin-polarized fermions are a collisionless gas⁶⁹, which in a purely harmonic trap has its lowest parametric resonance for motion along the y axis at $2\omega_y^F$. The energy and spectral width of the fermions' spectral response is obtained using a fit to a phenomenological function (Fig. 1c and Supplementary Information). The broad fan below $2\omega_y^F$ visible in the fermionic response (Fig. 1b) arises from strong driving in an anharmonic trap (Supplementary Information).

Figure 2 shows a selection of the bosons' and fermions' spectral response for various interspecies coupling strengths. The resonances of the BEC are always well described by the hydrodynamic scaling

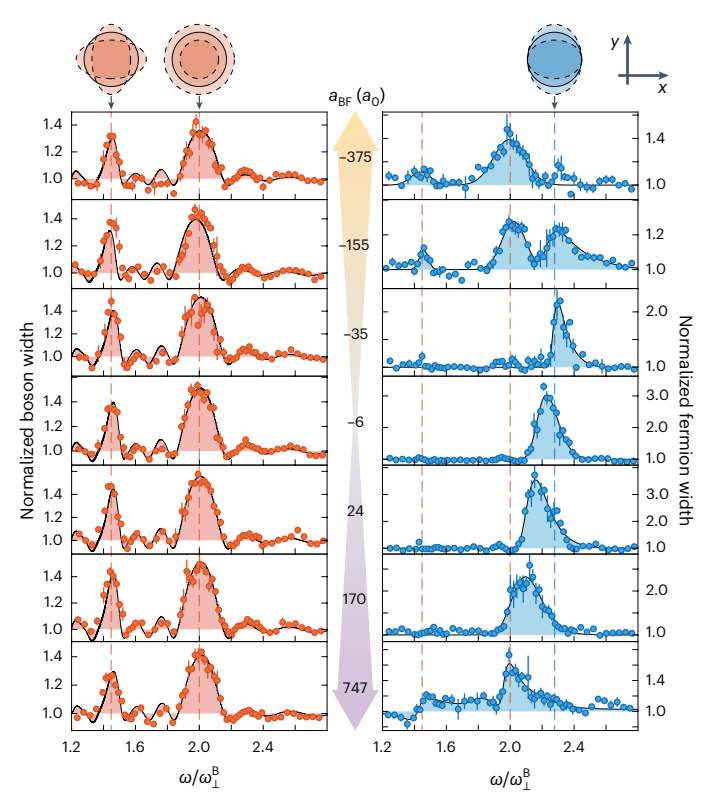


Fig. 2 | **Evolution of Bose–Fermi collective modes across varying interaction strength.** Illustrations depict the oscillations of the cloud's transverse (x-y) cross-section. The boson quadrupole and breathing modes (shown in red) lie at $\sqrt{2}\omega_{\perp}^{\rm B}$ and $2\omega_{\perp}^{\rm B}$, respectively, whereas the fermions' transverse resonance in the collisionless regime lies at $2\omega_y^{\rm F}$ (shown in blue). The spectra depict bosonic and fermionic cloud widths (circles) for varying modulation frequencies. As $a_{\rm BF}$ increases towards either repulsive or attractive interactions, the fermion spectra evolve to mode lock to the BEC's superfluid hydrodynamic modes. An extended dataset can be found in Supplementary Information.

ansatz from equation (1). The BEC spectrogram is unaffected by interactions with the much more dilute gas of fermionic impurities. By contrast, the response of the fermions shows a strong dependence on the interspecies coupling strength. At weak couplings, the collisionless mode of the fermions shifts linearly with a_{BF} . With increasing interactions strengths, the fermionic response changes drastically, revealing two additional modes in the their spectral response that coincide with the BEC's hydrodynamic superfluid modes at $2\omega_{\perp}^{\rm B}$ and $\sqrt{2}\omega_{\perp}^{\rm B}$. All three modes are spectrally well resolved and show no broadening beyond the Fourier limit, in contrast to the broadened profiles that would arise from momentum-relaxing collisions (Supplementary Information). This is remarkable, given that the mean-free path for collisions changes from infinity at zero interaction strength to $l_{\rm mfp} = (4\pi a_{\rm BF}^2 n_{\rm B})^{-1} \approx 0.6 \,\mu{\rm mat}$ the strongest measured interactions, much shorter than the radial system size $L \approx 10 \mu m$. A thermal mixture would thus cross over from collisionless to collisionally hydrodynamic behaviour through an intermediate regime of strong damping. Here, instead, the fermions remain collisionless with the condensed bosons and, for the strongest interactions, even 'copy' the BEC's superfluid collective modes, not unlike dye particles in water.

The fermion collective modes are summarized in Fig. 3. For scattering lengths beyond $|a_{\rm BF}| > 350 a_0$ (with a_0 being the Bohr radius), the fermions exclusively respond at the BEC's hydrodynamic superfluid modes and show no signal of their own collisionless mode. For weaker interactions, we observe a mean-field-like shift of the fermion frequency proportional to the sign of the interaction, which for repulsive interactions merges with the BEC's breathing mode at $2\omega_1^{\rm B}$ and becomes

spectrally indistinguishable. We note that at repulsive interactions above $170a_0$ we observe a dispersive—rather than absorptive—feature in the fermionic response at the BEC quadrupole mode (Fig. 2 and extended dataset Supplementary Information). This Fano-type behaviour can be understood from coherent coupling of the fermionic and bosonic mode⁷⁰. At interactions stronger than measured here, ~900 a_0 , phase separation is predicted to occur²² (Supplementary Information).

To understand the dynamics across all interaction strengths, we compare various numerical models to the data. The linear dependence of the fermionic collisionless mode at weak interaction strengths qualitatively agrees with a mean-field description, considering the effective potential experienced by the fermions immersed in the Bose gas. The BEC in the Thomas–Fermi approximation takes on the shape of the inverted optical potential. The fermions thus experience a joint effective potential comprising the optical trap and the mean-field potential of the BEC, where attractive (repulsive) interspecies interactions provide a steeper (shallower) potential that shifts the trapping frequencies according to $\tilde{\omega}^2 = \omega_y^{\rm F^2} \left(1 - \frac{g_{\rm BF} \alpha_{\rm B}}{g_{\rm BB} \alpha_{\rm F}}\right)$ (Supplementary Infor-

mation). Here, $g_{\rm BF}=2\pi\hbar^2a_{\rm BF}/m_{\rm red}$ is the Bose–Fermi coupling strength, $m_{\rm red}=m_{\rm F}m_{\rm B}/(m_{\rm F}+m_{\rm B})$ is the reduced mass, $g_{\rm BB}=4\pi\hbar^2a_{\rm BB}/m_{\rm B}$ is the Bose–Bose coupling and $\alpha_{\rm B(F)}$ is the boson (fermion) optical polarizability. Qualitatively, this mean-field model (Fig. 3, dashed red line) shares the trend of the measurements for small $a_{\rm BF}$, but with a different slope. It also fails to predict the appearance of additional modes in the fermionic spectral response. To capture the resonances that fermions inherit from the BEC's superfluid hydrodynamic modes, the mean-field potential itself must properly incorporate the bosons' response given by the scaling ansatz equation (1).

We therefore turn to the full dynamics of the fermions as described by the Boltzmann–Vlasov equation

$$\frac{\partial f}{\partial t} + \frac{\mathrm{d}\mathbf{r}}{\mathrm{d}t} \frac{\partial f}{\partial \mathbf{r}} + \frac{\mathrm{d}\mathbf{p}}{\mathrm{d}t} \frac{\partial f}{\partial \mathbf{p}} = I_{\text{coll}},$$
(2)

where f is the fermion distribution at momentum \mathbf{p} and position \mathbf{r} , and I_{coll} is the collision integral. Anticipating the absence of collisions for fermions only interacting with the BEC, in the absence of thermal excitations, we set $I_{\text{coll}} = 0$. Then, to first order in g_{BF} , we derive a scaling ansatz for the fermions' width, assuming a harmonic trap and fermionic impurities that are deeply immersed in the BEC^{43,68,71}:

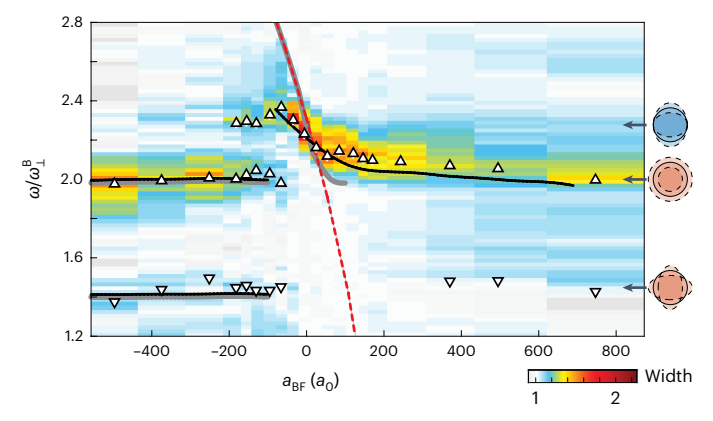
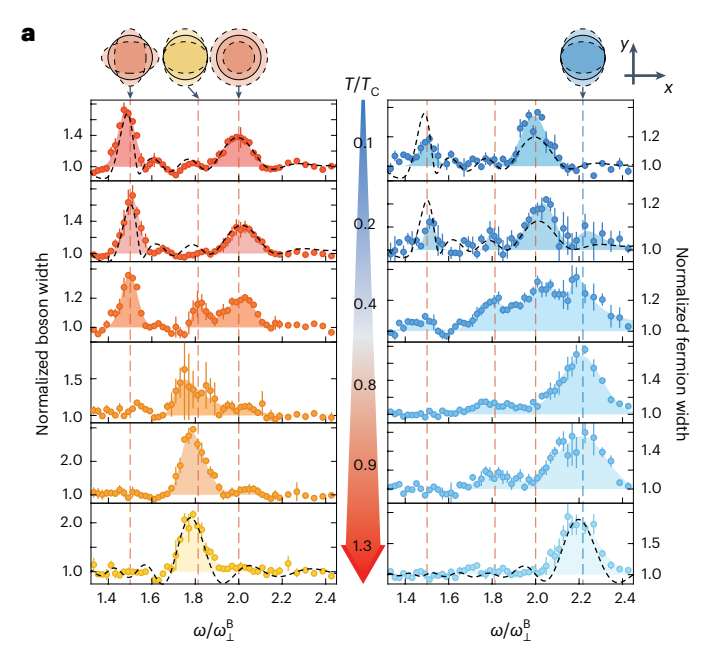


Fig. 3 | **Fermionic mode frequencies versus interspecies interaction.** The colour density plot displays the power spectra of cloud widths. The white markers denote the peak frequencies. The arrows on the right side indicate the three modes of Fig. 2. The dashed red line shows the naive mean-field prediction, and the grey lines are the scaling ansatz solution of the mean-field model equation (3). The black lines show the dominant modes of the collisionless Boltzmann–Vlasov solution accounting for finite system size and trap anharmonicity (Supplementary Information).



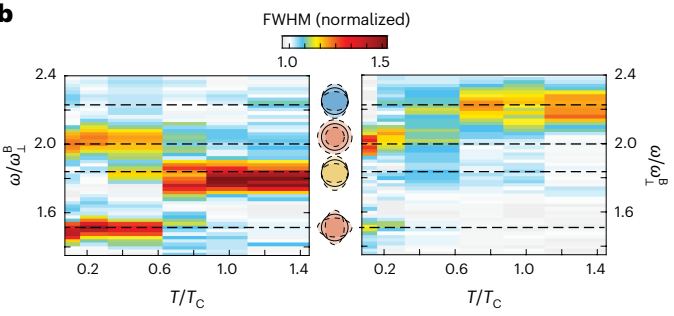


Fig. 4 | **Temperature dependence of the bosonic and fermionic collective modes at** $a_{BF} = -400a_0$. **a**, Spectrograms of the boson (left) and fermion (right) widths, as a function of the bosons' reduced temperature T/T_c . Top cartoons illustrate the bosonic hydrodynamic (red) and collisionless (yellow) modes and the fermionic collisionless (blue) modes. Peak boson densities for increasing T/T_c are $n_B = (7.3, 5.9, 5.4, 2.3, 1.4, 0.07) \times 10^{13}$ cm⁻³, respectively. The fermion spectrograms indicate hydrodynamic response at the BEC's quadrupole and breathing mode frequencies for the lowest temperatures. The dashed lines in the upmost panels for $T/T_c \approx 0.1$ and $T/T_c \approx 0.2$ represent the theoretical prediction based on the scaling ansatz for the BEC dynamics and Boltzmann–Vlasov equation for the dynamics of fermions. Dashed lines for $T > T_c$ show the result of solving coupled Bose–Fermi Boltzmann equations (Supplementary Information). **b**, Summary of the obtained peak frequencies for bosons (left) and fermions (right), with the colour indicating the spectral response. FWHM, full-width at half-maximum.

$$\ddot{c}_{i} + \omega_{i,\text{eff}}^{F}(t)^{2} c_{i} - \left(1 - \frac{g_{BF} \alpha_{B}}{g_{BB} \alpha_{F}}\right) \frac{\omega_{j}^{F}(0)^{2}}{c_{i}^{3}} = 0$$
with $\omega_{i,\text{eff}}^{F}(t)^{2} = \left(1 - \frac{g_{BF} \alpha_{B}}{g_{BB} \alpha_{F}}\right) \omega_{i}^{F}(t)^{2} - \frac{g_{BF}}{g_{BB}} \frac{b_{i}}{b_{i}}$ (3)

Here, c_i is the dimensionless scaling parameter of the width of the gas of fermionic impurities, with $c_i(t=0)=1$. This ansatz (shown in grey lines) captures the fermionic response to the BEC's superfluid mode on the attractive side (Supplementary Information), which can thus indeed be explained as the collisionless flow of fermions experiencing the coherent interactions with the BEC. The simple ansatz fails for repulsive interactions above $a_{\rm BF} > 100 a_0$ where the mean-field potential is strong enough to repel fermions from the BEC. A full numerical simulation of the collisionless Boltzmann–Vlasov equation (Supplementary

Information)—including the temperature-dependent fermionic cloud size and the trap anharmonicity—is shown as the solid black line in Fig. 3, which accurately captures all of the observed modes across all interaction strengths, validating our neglect of the collisional term in equation (2).

Indeed, collisionless flow is expected for the impurities well below the bosons' superfluid transition temperature, as fermions slower than the condensate's speed of sound (~5 µm ms⁻¹) can only dissipate energy through collisions with thermal bosons, which are essentially absent at low temperatures $T/T_c \approx 0.2$. To measure the impact of collisions of fermions with thermal bosons, we now probe the mixture at increasing temperatures across the BEC phase transition. The physics is complex already for bosons alone, as the BEC becomes immersed in a cloud of thermal excitations, and the thermal cloud's collective modes couple to those of the superfluid⁶⁷. We employ the same protocol as before, using a drive that couples strongly to the BEC's quadrupole mode (Supplementary Information). The relative temperature T/T_c is varied at a fixed scattering length $a_{BF} = -400a_0$ by reducing the number of bosons while fixing the same final temperature. The radial trap ellipticity (Supplementary Information) allows us to distinguish the collisionless mode of the bosons' thermal component at $2\omega_{\nu}^{\rm B}$ from the superfluid breathing mode at $2\omega_{\perp}^{B}$, as depicted in Fig. 4a. Figure 4b displays the change of the bosons' and fermions' spectral responses with temperature. At low temperatures, the bosons exhibit resonances at the BEC quadrupole $(\sqrt{2}\omega_{\perp}^{\rm B})$ and breathing $(2\omega_{\perp}^{\rm B})$ modes. At $T > 0.5T_{\rm c}$ we observe an additional peak at $2\omega_{\nu}^{\rm B}$, corresponding to the intraspecies collisionless mode of the bosonic thermal component^{53,54}. With increasing T/T_{cr} the bosonic response at the BEC superfluid modes is reduced while the response at the intraspecies collisionless mode grows, until above T_c only the collisionless mode persists.

The fermions can be viewed as a highly sensitive probe for the complex crossover of modes in the Bose gas. At the coldest temperatures, they respond exclusively at the frequencies of the BEC's hydrodynamic modes. Remarkably, starting at $T/T_c \approx 0.4$, two additional modes appear in the fermionic response. The lower resonance at $2\omega_y^B$ coincides with the intraspecies collisionless mode of the bosonic thermal component whereas the higher one at $2\omega_y^F$ coincides with the native collisionless mode of the fermions. Above T_c , the fermions respond only at their collisionless mode at $2\omega_y^F$, and this regime is well captured by solving the full coupled Boltzmann equations for the mixture with non-vanishing $I_{\rm coll}$ (Supplementary Information and ref. 70). We note that, while the thermal components of the bosons and the spin-polarized fermions are both in the collisionless regime by themselves, strong interspecies interactions bring this mixture into local equilibrium 63 . We interpret the fermionic response at the bosonic

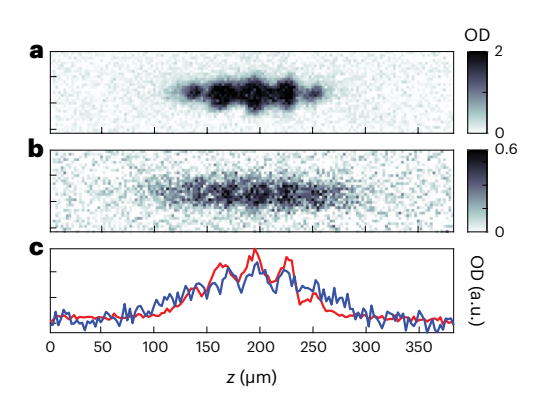


Fig. 5 | **Faraday waves in a Bose–Fermi mixture. a,b**, In situ absorption images show the longitudinal density pattern in the BEC (**a**) and the fermions (**b**), at an interspecies interaction of $500a_0$. Bose–Fermi interactions cause the BEC density striation to be imprinted on the fermions, as seen in the optical densities (OD). **c**, Line densities for the bosons (red) and fermions (blue), with the fermions rescaled by a factor of 3 for easier comparison.

collisionless mode $(0.3T_c \lesssim T \lesssim T_c)$ as an indication of the mixture's crossover from the collisionless to the collisionally hydrodynamic regime. Above T_c , the mixture reverts to collisionless flow for both species due to the lowered density of bosons.

The quadrupole and breathing modes are low-lying collective excitations of the coupled system, but perhaps the most visually striking observation of synchronized flow is the appearance of high-order excitations-Faraday waves⁷²-in the Bose-Fermi mixture. They arise from the parametric excitation of collective modes transverse to the direction of drive. In the context of atomic gases, Faraday waves have been observed in elongated BECs⁷³⁻⁷⁵ upon modulating weakly interacting BECs along the radial direction, inducing striated density patterns along the longitudinal direction. Strikingly, when inducing Faraday waves in the BEC, we here observe the emergence of Faraday waves also on in the gas of fermions at $a_{RE} = 500a_0$ (Fig. 5). For this, we modulated the radial optical potential for eight cycles at $2\omega_r^B$. From the observed period of $\lambda_{\text{Far}} = 28(7) \, \mu \text{m in the density striction}$ and the drive frequency we infer the condensate's speed of sound $c = 5.5(1.4) \, \mu \text{m ms}^{-1}$, which is consistent with the Bogoliubov speed of sound obtained from the measured chemical potential μ , $c = \sqrt{\mu/m_{\rm B}} = 4.9(2) \,\mu{\rm m \, ms^{-1}}$. To our knowledge, this is the first observation of spatial patterns analogous to Faraday modes observed in a gas of fermions.

Our results demonstrate a novel regime of collective motion of fermions, tracing the superfluid hydrodynamic flow of a Bose condensate. As the temperature is increased, incoherent collisions between the thermal bosons and fermions cause a crossover into the collision-dominated hydrodynamic regime, in direct analogy to two-dimensional electron gases, where the electron mean-free path is tuned with the density and temperature. At temperatures lower than those achieved in this study, induced fermion–fermion interactions^{76,77} are predicted to arise within the Bose–Fermi mixture, a precursor of the long-sought p-wave superfluidity of fermions mediated by bosons^{78–80}.

Online content

Any methods, additional references, Nature Portfolio reporting summaries, source data, extended data, supplementary information, acknowledgements, peer review information; details of author contributions and competing interests; and statements of data and code availability are available at https://doi.org/10.1038/s41567-024-02541-w.

References

- Landau, L. D. The movement of electrons in the crystal lattice. Phys. Z. Sowjetunion 3, 644 (1933).
- Pekar, S. I. Autolocalization of the electron in an inertially polarizable dielectric medium. Zh. Eksp. Teor. Fiz. 16, 335 (1946).
- Ebner, C. & Edwards, D. The low temperature thermodynamic properties of superfluid solutions of ³He in ⁴He. *Phys. Rep.* 2, 77–154 (1971).
- Schaefer, B.-J. & Wambach, J. The phase diagram of the quark-meson model. Nucl. Phys. A 757, 479–492 (2005).
- Sidler, M. et al. Fermi polaron-polaritons in charge-tunable atomically thin semiconductors. Nat. Phys. 13, 255–261 (2017).
- Shimazaki, Y. et al. Strongly correlated electrons and hybrid excitons in a moiréheterostructure. *Nature* 580, 472–477 (2020).
- Schwartz, I. et al. Electrically tunable Feshbach resonances in twisted bilayer semiconductors. Science 374, 336–340 (2021).
- Hadzibabic, Z. et al. Two-species mixture of quantum degenerate Bose and Fermi gases. Phys. Rev. Lett. 88, 160401 (2002).
- Stan, C. A., Zwierlein, M. W., Schunck, C. H., Raupach, S. M. F. & Ketterle, W. Observation of Feshbach resonances between two different atomic species. *Phys. Rev. Lett.* 93, 143001 (2004).
- Inouye, S. et al. Observation of heteronuclear Feshbach resonances in a mixture of bosons and fermions. *Phys. Rev. Lett.* 93, 183201 (2004).

- Silber, C. et al. Quantum-degenerate mixture of fermionic lithium and bosonic rubidium gases. *Phys. Rev. Lett.* 95, 170408 (2005).
- Ospelkaus, S., Ospelkaus, C., Humbert, L., Sengstock, K. & Bongs, K. Tuning of heteronuclear interactions in a degenerate Fermi-Bose mixture. *Phys. Rev. Lett.* 97, 120403 (2006).
- Zaccanti, M. et al. Control of the interaction in a Fermi–Bose mixture. Phys. Rev. A 74, 041605 (2006).
- Shin, Y.-i, Schirotzek, A., Schunck, C. H. & Ketterle, W. Realization of a strongly interacting Bose–Fermi mixture from a two-component Fermi gas. *Phys. Rev. Lett.* 101, 070404 (2008).
- Wu, C.-H., Santiago, I., Park, J. W., Ahmadi, P. & Zwierlein, M. W. Strongly interacting isotopic Bose–Fermi mixture immersed in a Fermi sea. *Phys. Rev. A* 84, 011601 (2011).
- Park, J. W. et al. Quantum degenerate Bose–Fermi mixture of chemically different atomic species with widely tunable interactions. *Phys. Rev. A* 85, 051602 (2012).
- 17. Vaidya, V. D., Tiamsuphat, J., Rolston, S. L. & Porto, J. V. Degenerate Bose–Fermi mixtures of rubidium and ytterbium. *Phys. Rev. A* **92**, 043604 (2015).
- Trautmann, A. et al. Dipolar quantum mixtures of erbium and dysprosium atoms. Phys. Rev. Lett. 121, 213601 (2018).
- Lous, R. S. et al. Probing the interface of a phase-separated state in a repulsive Bose–Fermi mixture. *Phys. Rev. Lett.* 120, 243403 (2018).
- DeSalvo, B. J., Patel, K., Cai, G. & Chin, C. Observation of fermionmediated interactions between bosonic atoms. *Nature* 568, 61–64 (2019).
- Patel, K., Cai, G., Ando, H. & Chin, C. Sound propagation in a Bose–Fermi mixture: from weak to strong interactions. *Phys. Rev. Lett.* 131, 083003 (2023).
- Viverit, L., Pethick, C. J. & Smith, H. Zero-temperature phase diagram of binary boson–fermion mixtures. *Phys. Rev. A* 61, 053605 (2000).
- 23. Büchler, H. P. & Blatter, G. Supersolid versus phase separation in atomic Bose-Fermi mixtures. *Phys. Rev. Lett.* **91**, 130404 (2003).
- Bertaina, G., Fratini, E., Giorgini, S. & Pieri, P. Quantum Monte Carlo study of a resonant Bose–Fermi mixture. *Phys. Rev. Lett.* 110, 115303 (2013).
- Kinnunen, J. J. & Bruun, G. M. Induced interactions in a superfluid Bose–Fermi mixture. *Phys. Rev. A* 91, 041605 (2015).
- Ludwig, D., Floerchinger, S., Moroz, S. & Wetterich, C. Quantum phase transition in Bose-Fermi mixtures. *Phys. Rev. A* 84, 033629 (2011).
- 27. Ferrier-Barbut, I. et al. A mixture of Bose and Fermi superfluids. Science **345**, 1035–1038 (2014).
- Delehaye, M. et al. Critical velocity and dissipation of an ultracold Bose-Fermi counterflow. Phys. Rev. Lett. 115, 265303 (2015).
- Yao, X.-C. et al. Observation of coupled vortex lattices in a mass-imbalance Bose and Fermi superfluid mixture. Phys. Rev. Lett. 117, 145301 (2016).
- 30. Roy, R., Green, A., Bowler, R. & Gupta, S. Two-element mixture of Bose and Fermi superfluids. *Phys. Rev. Lett.* **118**, 055301 (2017).
- Wu, Y. P. et al. Coupled dipole oscillations of a mass-imbalanced Bose–Fermi superfluid mixture. Phys. Rev. B 97, 020506 (2018).
- Ospelkaus, C., Ospelkaus, S., Sengstock, K. & Bongs, K. Interaction-driven dynamics of ⁴⁰K–⁸⁷Rb fermion–boson gas mixtures in the large-particle-number limit. *Phys. Rev. Lett.* 96, 020401 (2006).
- Huang, B. et al. Breathing mode of a Bose–Einstein condensate repulsively interacting with a fermionic reservoir. *Phys. Rev. A* 99, 041602 (2019).
- 34. Hu, M.-G. et al. Bose polarons in the strongly interacting regime. *Phys. Rev. Lett.* **117**, 055301 (2016).
- Yan, Z. Z., Ni, Y., Robens, C. & Zwierlein, M. W. Bose polarons near quantum criticality. Science 368, 190–194 (2020).

- Landau, L. D. Two-fluid model of liquid helium II. J. Phys. USSR 5, 71–90 (1941).
- Chevy, F. Counterflow in a doubly superfluid mixture of bosons and fermions. *Phys. Rev. A* 91, 063606 (2015).
- Seetharam, K., Shchadilova, Y., Grusdt, F., Zvonarev, M. B. & Demler, E. Dynamical quantum Cherenkov transition of fast impurities in quantum liquids. *Phys. Rev. Lett.* 127, 185302 (2021).
- Seetharam, K., Shchadilova, Y., Grusdt, F., Zvonarev, M. & Demler, E. Quantum Cherenkov transition of finite momentum Bose polarons. Preprint at https://arxiv.org/abs/2109.12260 (2021).
- Miyakawa, T., Suzuki, T. & Yabu, H. Sum-rule approach to collective oscillations of a boson–fermion mixed condensate of alkali-metal atoms. *Phys. Rev. A* 62, 063613–063611 (2000).
- 41. Yip, S. K. Collective modes in a dilute Bose–Fermi mixture. *Phys. Rev. A* **64**, 023609 (2001).
- Sogo, T., Miyakawa, T., Suzuki, T. & Yabu, H. Random-phase approximation study of collective excitations in the Bose–Fermi mixed condensate of alkali-metal gases. *Phys. Rev. A* 66, 136181– 1361812 (2002).
- Liu, X. J. & Hu, H. Collisionless and hydrodynamic excitations of trapped boson-fermion mixtures. Phys. Rev. A 67, 023613 (2003).
- Capuzzi, P., Minguzzi, A. & Tosi, M. P. Collisional oscillations of trapped boson–fermion mixtures in the approach to the collapse instability. *Phys. Rev. A* 69, 053615 (2004).
- Imambekov, A. & Demler, E. Exactly solvable case of a onedimensional Bose–Fermi mixture. Phys. Rev. A 73, 021602 (2006).
- Banerjee, A. Dipole oscillations of a Bose–Fermi mixture: effect of unequal masses of Bose and Fermi particles. J. Phys. B 42, 235301 (2009).
- 47. Van Schaeybroeck, B. & Lazarides, A. Trapped phase-segregated Bose-Fermi mixtures and their collective excitations. *Phys. Rev. A* **79**, 033618 (2009).
- Maruyama, T., Yamamoto, T., Nishimura, T. & Yabu, H. Deformation dependence of breathing oscillations in Bose–Fermi mixtures at zero temperature. J. Phys. B 47, 25–34 (2014).
- Asano, Y., Narushima, M., Watabe, S. & Nikuni, T. Collective excitations in Bose-Fermi mixtures. J. Low Temp. Phys. 196, 133–139 (2019).
- 50. Ono, Y., Hatsuda, R., Shiina, K., Mori, H. & Arahata, E. Three sound modes in a Bose–Fermi superfluid mixture at finite temperatures. *J. Phys. Soc. Jpn* **88**, 034003 (2019).
- Zhang, J. et al. Anomalous thermal diffusivity in underdoped YBa₂Cu₃O_{6+x}. Proc. Natl Acad. Sci. USA 114, 5378–5383 (2017).
- Gooth, J. et al. Thermal and electrical signatures of a hydrodynamic electron fluid in tungsten diphosphide. *Nat. Commun.* 9, 4093 (2018).
- Jin, D. S., Ensher, J. R., Matthews, M. R., Wieman, C. E. & Cornell, E. A. Collective excitations of a Bose–Einstein condensate in a dilute gas. *Phys. Rev. Lett.* 77, 420–423 (1996).
- Mewes, M. O. et al. Collective excitations of a Bose–Einstein condensate in a magnetic trap. Phys. Rev. Lett. 77, 988–991 (1996).
- Stamper-Kurn, D. M., Miesner, H. J., Inouye, S., Andrews, M. R.
 Ketterle, W. Collisionless and hydrodynamic excitations of a Bose-Einstein condensate. *Phys. Rev. Lett.* 81, 500–503 (1998).
- Gensemer, S. D. & Jin, D. S. Transition from collisionless to hydrodynamic behavior in an ultracold Fermi gas. *Phys. Rev. Lett.* 87, 173201 (2001).
- 57. O'Hara, K. M., Hemmer, S. L., Gehm, M. E., Granade, S. R. & Thomas, J. E. Observation of a strongly interacting degenerate Fermi gas of atoms. *Science* **298**, 2179–2182 (2002).
- 58. Regal, C. A. & Jin, D. S. Measurement of positive and negative scattering lengths in a Fermi gas of atoms. *Phys. Rev. Lett.* **90**, 230404 (2003).
- Bourdel, T. et al. Measurement of the interaction energy near a Feshbach resonance in a ⁶Li Fermi gas. *Phys. Rev. Lett.* 91, 020402 (2003).

- Trenkwalder, A. et al. Hydrodynamic expansion of a strongly interacting Fermi–Fermi mixture. *Phys. Rev. Lett.* **106**, 115304 (2011).
- 61. Tey, M. K. et al. Collective modes in a unitary Fermi gas across the superfluid phase transition. *Phys. Rev. Lett.* **110**, 055303 (2013).
- Ravensbergen, C. et al. Resonantly interacting Fermi–Fermi mixture of ¹⁶¹Dy and ⁴⁰K. Phys. Rev. Lett. **124**, 203402 (2020).
- 63. Ferlaino, F. et al. Dipolar oscillations in a quantum degenerate Fermi-Bose atomic mixture. *J. Opt. B* **5**, S3–S8 (2003).
- 64. Fukuhara, T., Tsujimoto, T. & Takahashi, Y. Quadrupole oscillations in a quantum degenerate Bose–Fermi mixture. *Appl. Phys. B* **96**, 271–274 (2009).
- 65. Kagan, M. Y. & Bianconi, A. Fermi-Bose mixtures and BCS-BEC crossover in high-T_c superconductors. *Condens. Matter* **4**, 51 (2019).
- Stringari, S. Collective excitations of a trapped Bose-condensed gas. Phys. Rev. Lett. 77, 2360–2363 (1996).
- 67. Pethick, C. & Smith, H. Bose–Einstein Condensation in Dilute Gases (Cambridge Univ. Press, 2008).
- 68. Castin, Y. & Dum, R. Bose-Einstein condensates in time dependent traps. *Phys. Rev. Lett.* **77**, 5315–5319 (1996).
- DeMarco, B., Bohn, J. L., Burke, J. P., Holland, M. & Jin, D. S. Measurement of p-wave threshold law using evaporatively cooled fermionic atoms. *Phys. Rev. Lett.* 82, 4208–4211 (1999).
- Dolgirev, P. E. et al. Accelerating analysis of Boltzmann equations using Gaussian mixture models: application to quantum Bose–Fermi mixtures. Preprint at https://arxiv.org/abs/2304.09911 (2022).
- 71. Menotti, C., Pedri, P. & Stringari, S. Expansion of an interacting Fermi gas. *Phys. Rev. Lett.* **89**, 250402 (2002).
- Faraday, M. On a peculiar class of acoustical figures; and on certain forms assumed by groups of particles upon vibrating elastic surfaces. *Phil. Trans. R. Soc. Lond.* 121, 299–340 (1831).
- Engels, P., Atherton, C. & Hoefer, M. A. Observation of Faraday waves in a Bose–Einstein condensate. *Phys. Rev. Lett.* 98, 095301 (2007).
- 74. Groot, A. Excitations in Hydrodynamic Ultra-Cold Bose Gases. PhD thesis, Utrecht Univ. (2015).
- 75. Nguyen, J. H. et al. Parametric excitation of a Bose–Einstein condensate: from Faraday waves to granulation. *Phys. Rev. X* **9**, 11052 (2019).
- Heiselberg, H., Pethick, C. J., Smith, H. & Viverit, L. Influence of induced interactions on the superfluid transition in dilute Fermi gases. *Phys. Rev. Lett.* 85, 2418–2421 (2000).
- 77. Bijlsma, M. J., Heringa, B. A. & Stoof, H. T. Phonon exchange in dilute Fermi–Bose mixtures: tailoring the Fermi–Fermi interaction. *Phys. Rev. A* **61**, 053601 (2000).
- Efremov, D. V. & Viverit, L. p-wave Cooper pairing of fermions in mixtures of dilute Fermi and Bose gases. *Phys. Rev. B* 65, 134519 (2002).
- 79. Matera, F. Fermion pairing in Bose–Fermi mixtures. *Phys. Rev. A* **68**, 043624 (2003).
- 80. Kinnunen, J. J., Wu, Z. & Bruun, G. M. Induced p-wave pairing in Bose-Fermi mixtures. *Phys. Rev. Lett.* **121**, 253402 (2018).

Publisher's note Springer Nature remains neutral with regard to jurisdictional claims in published maps and institutional affiliations.

Springer Nature or its licensor (e.g. a society or other partner) holds exclusive rights to this article under a publishing agreement with the author(s) or other rightsholder(s); author self-archiving of the accepted manuscript version of this article is solely governed by the terms of such publishing agreement and applicable law.

© The Author(s), under exclusive licence to Springer Nature Limited 2024

Methods

Here we provide further details of the collective oscillation measurements. The optical potential is generated by two 1,064 nm beams intersecting at 90°, oriented in the zand y directions, respectively. The trap is approximately cylindrically symmetric with trap frequencies of $\omega_{x,y,z}^B/2\pi = [103(3), 94(2), 12.2(0.3)]$ Hz and $\omega_{x,y,z}^F/2\pi = [125(2), 114(2), 15(1)]$ Hz for bosons and fermions, which are prepared in their respective hyperfine ground states ($|F=1,m_F=1\rangle$ for 23 Na and $|F=9/2,m_F=-9/2\rangle$ for 40 K). The fermions are moderately degenerate with T/T_F ranging from 0.6 to 2, where T_F is the Fermi temperature. The large variation stems from mean-field attraction and repulsion as well as different degrees of three-body inelastic loss that removes the minority fermions when $|a_{BF}|$ is large. The BEC is weakly interacting with a Bose–Bose scattering length of $a_{BB}=52a_0$, where a_0 is the Bohr radius. Our lowest temperatures are $T/T_c\lesssim 0.2$ with respect to the BEC critical temperature T_c .

To create an interacting Bose-Fermi mixture, we ramp the magnetic field in between two interspecies Feshbach resonances, allowing continuous tuning of the interspecies s-wave scattering length, a_{BF} . First, we ramp the magnetic field to the zero crossing of the scattering length at 80.3 G and wait for the field to stabilize for 5 ms. Then, the field is quenched to the final interaction strength within 10 µs, and oscillations are initiated. We take care to feed forward the programming of the magnetic field to compensate for slower drifts of eddy currents on the several-millisecond timescales. We check the field is stable during the oscillation perturbation sequence by independently measuring it using radiofrequency spectroscopy on the impurity atoms. During the oscillations, differential gravitational sag between the species is cancelled using a magnetic field gradient. To centre the two species, we empirically found the correct magnetic gradient by minimizing the lifetime of the K atoms at strong interactions with the Na atoms as a function of gradient value. At the best overlap point, the K atoms underwent the fastest inelastic three-body losses with Na atoms. The density overlap profiles may be found in the supplementary section on equilibrium line densities in Supplementary Information.

We study the collective modes versus interaction strength at a fixed $T/T_c \approx 0.2$ (Fig. 2) by applying a sinusoidal intensity perturbation on the z-axis 1,064 nm trap beam with a modulation amplitude of 20% and a variable drive frequency. This method injects energy in the x and y motion of the clouds and primarily excites the transverse breathing mode. We study the collective modes versus temperature at a fixed interaction strength (set by the scattering length $a_{BF} = -400a_0$) by applying intensity modulations to both the z- and y-directional 1,064 nm beams (Fig. 4). The modulation in each direction is 180° out of phase in order to better couple to the transverse quadrupole mode. The modulation depths are 15% for both beams. In both cases, the clouds are imaged after a duration lasting ten oscillation cycles. To minimize power broadening of the spectra and maximize the Fourier resolution, the modulation amplitude is minimized and the number of cycles is maximized within the experimental limits of signal-to-noise ratio and lifetime from inelastic collisions. Our chosen modulation depth is strong enough that the oscillations slightly deviate from linear

To study the evolution of collective modes versus temperature, we reduced the evaporation efficiency of the mixture by ramping the optical potential to its final value more quickly, leading to a similar absolute temperature but reduced boson number.

Fitting of the fermion spectrograms, that is, in Fig. 1, is performed with a phenomenological asymmetric function of the form

$$c(\omega, p_i) = \frac{p_1}{f(\omega, p_2, p_3, p_4)} e^{-(\omega - p_2)^2 / f(p_2, p_3, p_4)^2},$$
with $f(\omega, p_2, p_3, p_4) = p_3 (1 + e^{p_4(\omega - p_2)})^{-1}$, (4)

with p_i as free fitting parameters. This function reduces to a Gaussian in the limit $p_4 = 0$, and only the peak location and width are used in data analysis. The asymmetry and downshifting of the non-interacting fermion resonance from its expected frequency is due to strong driving of the fermions in an anharmonic trap.

In Figs. 1–4, the modulation frequencies are shown as normalized to the boson mean radial trap frequency, $\omega_{\perp}^{\rm B}$, which is $2\pi \times 98$ Hz on average. However, long-term drifts of the trap depth over many experimental repetitions necessitated a different normalization for each interaction strength in Figs. 2 and 3. The exact normalization value was determined by fitting a Gaussian to the boson spectrograms at frequencies near $\omega_{\perp}^{\rm B}$, extracting the frequency of the largest response and assigning that as the normalization for the boson and fermion spectograms for that particular $a_{\rm BF}$. This procedure necessarily forces the BEC breathing mode in Fig. 2 to fall at $2\omega_{\perp}^{\rm B}$, and falls to the same absolute frequency to within 2% error for all driving conditions.

Data availability

The data that support the plots within this paper and other findings of this study are available as source data files. All other data are available from the corresponding author upon reasonable request.

Acknowledgements

We acknowledge E. Wolf for helpful discussions. We acknowledge support from NSF, AFOSR through a MURI on Ultracold Molecules, the Vannevar Bush Faculty Fellowship. Z.Z.Y. and A.C. acknowledge support from the NSF GRFP. C.R. acknowledges support from the Deutsche Forschungsgemeinschaft (DFG) Germany research fellowship (421987027). K.S. acknowledges funding from NSF EAGER-QAC-QCH award no. 2037687. P.D. and E.D. were supported by ARO grant number W911NF-20-1-0163, SNSF project 200021-212899. E.D. acknowledges support from the Swiss National Science Foundation under Division II.

Author contributions

M.Z. and E.D. conceived of the experiments and supervised the study. Z.Z.Y., Y.N., A.C. and C.R. performed the experiments and the data analysis. Z.Z.Y., C.R. and M.Z. performed the numerical calculations for the Boltzmann equations without collisions and the mean-field scaling ansatz. P.E.D., K.S. and E.D. performed the theoretical and numerical calculations on the high-temperature Boltzmann equations. All authors contributed to the paper and the interpretation of data.

Competing interests

The authors declare no competing interests.

Additional information

Supplementary information The online version contains supplementary material available at https://doi.org/10.1038/s41567-024-02541-w.

Correspondence and requests for materials should be addressed to Martin Zwierlein.

Peer review information *Nature Physics* thanks Xing-Can Yao and the other, anonymous, reviewer(s) for their contribution to the peer review of this work.

Reprints and permissions information is available at www.nature.com/reprints.